ISSN: 1692-7257 - Volume 2 – Issue 48 - 2026

ORIGINAL

RCTA
Revista Colombiana de Tecnologías de Avanzada
UNIPAMPLONA

Electrodeposition and morphological characterization of NiSx coatings on nickel foam

Electrodeposición y caracterización morfológica de capas de NiSx sobre espuma de níquel

Claudia Patricia Parra Medina[1,2]
Edwin García Quintero[3]
Héctor Darío Sánchez Londoño[3]

[1] **Universidad de Antioquia, Facultad de Ingenierías, Programa de Doctorado en Ingeniería de Materiales, Medellín, Antioquia, Colombia.**
[2] **Universidad Militar Nueva Granada, Facultad de Ingenierías, Programa de Ingeniería en Mecatrónica, Bogotá D.C, Colombia.**
[3] **Universidad de Antioquia, Facultad de Ingenierías, Programa de Ingeniería Eléctrica, Medellín, Antioquia, Colombia.**

Received: 17 February 2026. Revised: 01 May 2026. Accepted: 23 June 2026. Published: 07 July 2026.
Corresponding Author: Claudia Patricia Parra Medina

How to cite: C. P. Parra Medina, E. García Quintero, and H. D. Sánchez Londoño, "Electrodeposición y caracterización morfológica de capas de NiSx sobre espuma de níquel", *Revista Colombiana de Tecnologías de Avanzada (RCTA)*, vol. 2, no. 48, jul. 2026, art. no. 4560, doi: 10.24054/rcta.v2i48.4560

This work is licensed under a Creative Commons Attribution-NonCommercial 4.0 International License.

Abstract:

This work evaluates two electrodeposition routes for obtaining nickel-sulfur (NiS_x) coatings on nickel foam substrates. The objective was to compare the effect of deposition conditions on surface morphology, coating thickness, and elemental Ni/S ratio of the resulting films. The first route was developed using potentiodynamic electrodeposition at a scan rate of 5 mV s^{-1}, between -0.54 and -1.44 V, for eight cycles. The second route was carried out using two current density steps, applying 10 mA cm^{-2} for 90 min and 100 mA cm^{-2} for 75 min. The resulting coatings were characterized by field emission scanning electron microscopy (FESEM) and energy-dispersive X-ray spectroscopy (EDX). Synthesis 1 produced a relatively uniform film with a fine granular morphology and lamellar growth associated with deposition cycles, with an average thickness of approximately 720 nm and a Ni/S atomic ratio close to 1:1. Synthesis 2 generated a cauliflower-like surface morphology, with a greater average thickness of approximately 700 nm and a Ni/S atomic ratio close to 2.5:1. These results show that the electrodeposition conditions significantly modify the microstructure, growth mode, and elemental composition of NiS_x coatings on nickel foam. This study provides useful experimental information for the design and optimization of nickel-sulfur films obtained by electrodeposition.

Keywords: electrodeposition; nickel sulfide; nickel foam; NiSx coatings; FESEM; EDX; surface morphology; Ni/S ratio.

Resumen:

En este trabajo se evaluaron dos rutas de electrodeposición para obtener recubrimientos de sulfuro de níquel, NiS_x, sobre sustratos de espuma de níquel. El objetivo fue comparar el efecto de las condiciones de deposición sobre la morfología superficial, el espesor del recubrimiento y la relación elemental Ni/S de las películas obtenidas. La primera ruta se desarrolló mediante electrodeposición potenciodinámica a una velocidad de barrido de 5 mV s^{-1}, entre -0.54 y -1.44 V, durante ocho ciclos. La segunda ruta se realizó mediante dos escalones de densidad de corriente, aplicando 10 mA cm^{-2} durante 90 min y 100 mA cm^{-2} durante 75 min. Los recubrimientos obtenidos fueron caracterizados mediante microscopía electrónica de barrido por emisión de campo, FESEM, y espectroscopía de energía dispersiva de rayos X, EDX. La síntesis 1 produjo una película relativamente uniforme, con morfología granular fina y crecimiento laminar asociado a los ciclos de deposición, con un espesor promedio aproximado de 720 nm y una relación atómica Ni/S cercana a 1:1. La síntesis 2 generó una morfología superficial tipo coliflor, con mayor espesor promedio aproximado de 700 nm y una relación atómica Ni/S cercana a 2.5:1. Estos resultados muestran que las condiciones de electrodeposición modifican de manera significativa la microestructura, el modo de crecimiento y la composición elemental de los recubrimientos NiS_x sobre espuma de níquel. El estudio aporta información experimental útil para el diseño y optimización de películas de sulfuro de níquel obtenidas por electrodeposición.

Palabras clave: electrodeposición, sulfuro de níquel; espuma de níquel; recubrimientos NiSx; FESEM; EDX; morfología superficial; relación Ni/S.

INTRODUCTION

Hydrogen production by water electrolysis has become established as an alternative of interest for the development of sustainable energy technologies, especially when coupled with electricity from renewable sources[1],[11]. However, the implementation of these systems still faces challenges related to the cost, availability, activity and stability of the materials used as electrodes, particularly under demanding operating conditions or in electrolytes containing aggressive species[1],[4],[11],[16], [21]–[24],[28].

Water electrolysis involves two main half-reactions: the hydrogen evolution reaction, HER, and the oxygen evolution reaction, OER. The OER is usually considered the most kinetically limiting process, owing to its multielectron mechanism and the participation of oxygenated intermediates adsorbed on the electrode surface [5]–[8]. For this reason, different families of transition-metal-based materials have been investigated, including oxides, hydroxides, oxyhydroxides, phosphides, sulfides, selenides and multicomponent heterostructures, as alternatives to noble-metal-based electrocatalysts[5],[9],[10], [12]–[19],[29],[31].

In particular, nickel-based materials have been widely studied because of their relative abundance, conductivity, compatibility with metallic substrates and ability to form active or precursor phases through electrochemical routes. Systems such as NiFe, NiFe-LDH, NiS_x, NiS and NiS_2 and related heterostructures have been reported as materials of interest in electrochemical applications, especially because of the possibility of modifying their morphology, composition and interface with the substrate[3],[4], [15]–[18],[20],[21],[24],[29],[30].

Operation in saline media or media associated with seawater electrolysis introduces additional challenges, owing to the presence of chloride ions, competition between anodic processes, the possible formation of chlorinated species and phenomena of corrosion or surface degradation of the electrode[1],[4],[11],[16], [21]–[24],[28]. This background justifies the general interest in developing materials supported on conductive substrates and with coatings capable of modifying the electrode surface. Nevertheless, to attribute HER activity, OER activity, selectivity or electrochemical stability, specific techniques such as voltammetry, polarization curves, electrochemical impedance, stability tests or product quantification are required. Consequently, in the present work this background is used only as technological context, not as evidence of the electrocatalytic performance of the films obtained.

Nickel foam is a three-dimensional substrate of interest for the growth of functional coatings, owing to its porous structure, electrical conductivity and surface availability for the nucleation of deposited materials. These characteristics have favored its use as a support for oxides, hydroxides, phosphides, sulfides and transition metal heterostructures [2]–[4],[15],[17],[20],[25],[30]. However, obtaining reproducible coatings on this type of substrate requires understanding how the synthesis conditions modify the morphology, thickness, continuity and elemental composition of the deposited layer.

Among the available synthesis routes, electrodeposition offers relevant advantages for the preparation of coatings on conductive substrates, since it allows controlling variables such as the applied potential, the current density, the scan rate, the deposition time, the number of cycles and the composition of the electrolytic bath[2],[18],[34],[35]. These variables influence the nucleation, growth, coalescence and compaction of the films, generating changes in the roughness, thickness, adhesion, growth mode and elemental composition of the coating. Therefore, electrodeposition is not only a manufacturing route for materials of functional interest, but also a useful strategy for studying the relationship between synthesis conditions and the microstructure of deposited films.

Nickel sulfides, NiS_x, belong to the family of transition metal chalcogenides and can present variable compositions, morphologies and Ni/S ratios depending on the synthesis method. Materials related to NiS, NiS_2, Ni_3S_2 and metal sulfide heterostructures have been reported, some of them supported on nickel foam or combined with other transition metal phases[3],[4],[17],[20], [24]–[26],[30]. Other chalcogenides and nanostructured materials, such as MoS_2, WSe_2 and hybrid systems, have also been studied in different electrochemical contexts, which shows the general interest in controlling the morphology and composition of this type of material [25]–[27].

Nevertheless, the identification of specific nickel sulfide phases requires complementary structural techniques, such as X-ray diffraction, XRD. For this reason, analyses based solely on field emission scanning electron microscopy, FESEM, and energy-dispersive X-ray spectroscopy, EDX, must be interpreted as morphological and compositional evidence, but not as definitive crystallographic confirmation of a particular phase. This distinction is important because the elemental Ni/S ratio obtained by EDX can suggest compositions compatible with certain nickel sulfide phases, but cannot by itself confirm the crystal structure of the coating.

The literature also shows that the morphological and compositional properties of nickel-based materials can depend significantly on the synthesis route employed. Strategies based on electrodeposition, heterostructure formation, interfacial modification and the construction of three-dimensional arrays have been developed to modify the surface of nickel-supported electrodes[2],[3],[15],[18],[20],[29],[30],[34],[35]. However, before discussing the functional performance

of these materials, the basic characteristics of the film formed must be clearly established, including deposit uniformity, thickness, growth mode, surface morphology and elemental composition.

In the field of previous work related to electrolysis, OER materials and electrode modification, different approaches have been reported to improve activity and stability through the incorporation of oxides, hydroxides, oxyhydroxides, phosphides, sulfides, interfacial layers or hierarchical structures[5],[9],[10], [13]–[18],[21],[22],[29],[31]. There is also background associated with the development of anodes for seawater electrolysis and with nanostructured materials derived from reduced graphene oxide or metal nanoparticles[32],[33]. These works serve as a general framework to highlight the importance of controlling the microstructure of coatings, although the scope of the present study is limited to the morphological and compositional characterization of electrodeposited NiS_x films.

Despite the advances reported in nickel-based materials and transition metal chalcogenides, more experimental information is still required on how different electrodeposition conditions modify the surface morphology, transverse growth, thickness and elemental Ni/S ratio of NiS_x coatings deposited directly on nickel foam. This information is relevant because the microstructure of the coating constitutes a prior step for any subsequent functional evaluation and allows synthesis criteria to be established before attributing specific electrochemical properties.

The gap addressed by this work focuses on comparing two electrodeposition routes to obtain NiS_x coatings on nickel foam under the same morphological and compositional characterization approach. The novelty of the study lies in contrasting a potentiodynamic route by cycles with a route by current density steps, evaluating how these conditions produce differences in the surface morphology, transverse growth mode, thickness and elemental Ni/S ratio of the films obtained.

Therefore, the objective of this work was to synthesize nickel sulfide coatings, NiS_x, on nickel foam by means of two electrodeposition routes and to compare the effect of the deposition conditions on the morphology, thickness, transverse growth and elemental composition of the films. The characterization was performed by FESEM and EDX. The main contribution of the manuscript consists of providing experimental evidence on the relationship between electrodeposition conditions, microstructure and Ni/S ratio in NiS_x films, as a basis for future structural and electrochemical studies.

THE EXPERIMENT

Two electrodeposition routes were evaluated to obtain nickel sulfide coatings, NiS_x, on nickel foam substrates. The purpose of this experimental stage was to compare the effect of the deposition conditions on the surface morphology, transverse growth, thickness and elemental composition of the films obtained. The nickel foam used had dimensions of 1 cm × 1 cm with a surface density of 420g/m^2. Table 1 summarizes the items, concentrations and electrodeposition conditions used for synthesis 1 and synthesis 2.

Table 1: Items and characteristics of each of the electrodepositions performed.

Synthesis No.	Items	Concen.	Electrodeposition characteristic
Synthesis 1	$Ni(NO_3)_2$	0.5 M	Rate=5mV/s with a $V_0 = -0.54V$ and $V_f = -1.44V$; 8 cycles were performed.
	$Na_2S_2O_3$	0.1M	
Synthesis 2	NaH_2PO_2	0.2M	Curr. Dens.1=10mA/cm^2 for 90 min Curr. Dens.2=100mA/cm^2 for 75 min
	$NiCl_2$	0.05M	
	$CS(NH_2)_2$	0.1 M	
	NH_4F	0.15M	

Source: own elaboration.

The electrodeposition of synthesis 1 and 2 was carried out using a two-electrode cell, employing nickel foam as the working electrode and SAE 316L stainless steel as the counter electrode, as shown in Figure 1a. Since a two-electrode configuration was used, the reported values correspond to the voltage applied between the working electrode and the counter electrode, and not to potentials measured against a reference electrode.

Before starting the electrodeposition process, the nickel foam was cleaned: the bare nickel foam was immersed in 1.0 M HCl for 20 min under sonication, then washed with ethanol and abundant deionized water and left to dry at room temperature. The clean nickel foam, with dimensions 1 cm x 1 cm and exposed geometric area of 1 cm^2, was immersed in the electrolyte and used as the working electrode.

The electrolyte for each electrodeposition was prepared as specified in Table 1 and stirred magnetically for approximately 25 minutes at room temperature (22 ± 2 °C). The electrodeposition of synthesis 1 was performed with a variable voltage source at a rate of 5 mV s^{-1} for 8 cycles, starting with a voltage of -0.54 V, up to -1.44 V.

After electrodeposition, the working electrodes were washed with deionized water and dried at room temperature. The mass of the deposited film was on average 1.5 mg cm^{-2}, determined from the mass difference of the nickel foam before and after electrodeposition. The electrodeposition of synthesis 2 was performed with the same source, using two current density steps of 10 mA cm^{-2} for 90 min and 100 mA cm^{-2} for 75 minutes, as shown in Figure 1b. After electrodeposition, the working

electrodes were washed with deionized water and dried at room temperature.

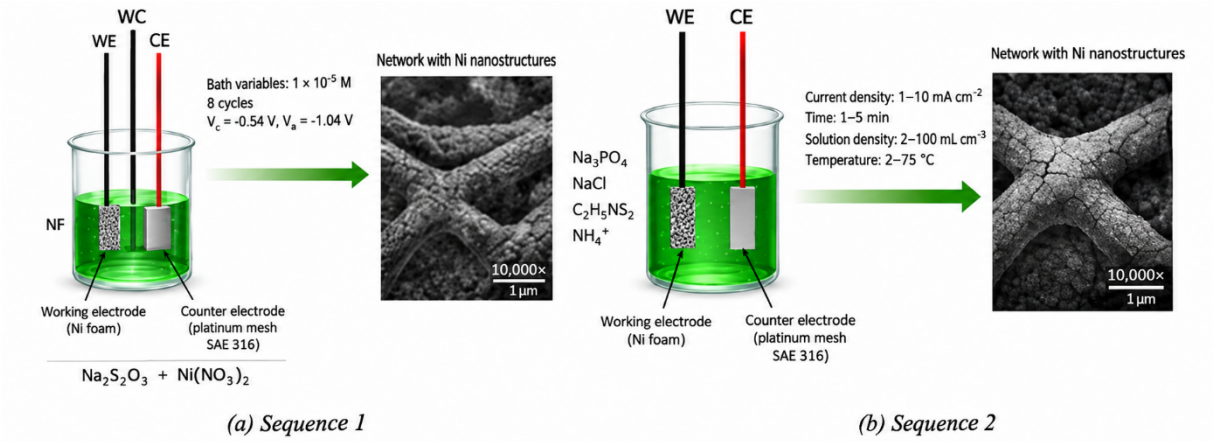

Fig. 1. *Electrodeposition scheme, (a). Synthesis 1 and (b). Synthesis 2.*
Source: Own elaboration.

The process was repeated 22 times for each synthesis route, yielding 22 specimens per experimental condition. From this set, representative samples were selected for FESEM-EDX based on the macroscopic integrity of the coating, the absence of visible detachment and surface continuity. Thickness and structure size measurements were performed in different areas of the available micrographs.

RESULTS AND DISCUSSION

Field emission scanning electron microscopy (FESEM) and energy-dispersive X-ray spectroscopy (EDX) were used to characterize the surface morphology, the cross section and the semiquantitative elemental composition of the electrodeposited NiS_x films.

Figure 2 shows the morphological characterization of Synthesis 1. Figure 2a shows the nickel foam coated with NiS_x. The micrograph was acquired with an accelerating voltage of 20.00 kV, a magnification of 200x and a probe current of 1.6 nA.

Figure 2b shows the NiSx layer on the nickel foam at an accelerating voltage of 20.00 kV with a magnification of 1000x and a probe current of 1.6 nA. The presence of cracked or fractured areas allowed the cross section of the coating to be observed and its thickness to be estimated. Figure 2c shows the surface morphology of the layer at an accelerating voltage of 5.00 kV with a magnification of 20,000x and a probe current of 0.2 nA; there, fine, rounded grain nanostructures with an average diameter of 180 nm. can be seen grown on the surface.

Figure 2d presents a close-up of the fractured area of the NiSx coating, at an accelerating voltage of 5.00 kV with a magnification of 30,000x and a probe current of 25 pA. From this micrograph, an average coating thickness of 720 nm was estimated.

In the cross section, a lamellar growth associated with the electrodeposition cycles is observed. The presence of eight sublayers is consistent with the eight cycles applied during synthesis 1. Figure 3 shows the lamellar growth of the coating and the formation of sublayers associated with the repetition of the electrodeposition cycles.

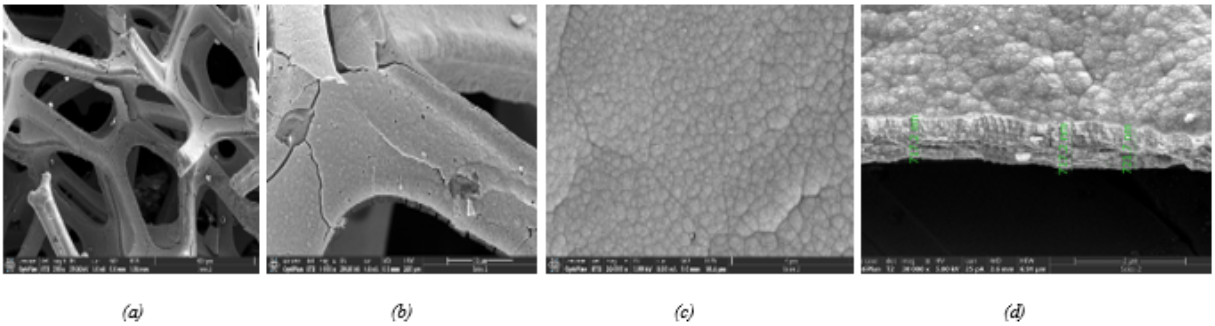

Fig. 2. *FESEM characterization of synthesis 1. (a). Nickel foam coated with NiSx, (b). NiSx layer, (c). Surface morphology of NiSx. (d). Thickness of the NiSx layer.*
Source: own elaboration.

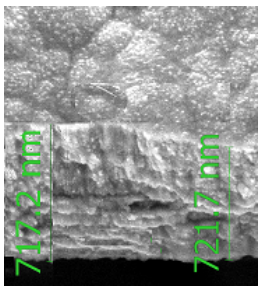

Source: own elaboration.

EDX microanalysis was performed on the coating obtained by synthesis 1, as shown in Figure 4. The microanalysis was performed in two representative regions: one located in the cross-sectional area of the lamellar coating and another on the film surface.

Figure 4a shows the points selected for the EDX analysis on the surface of the coating obtained by synthesis 1, while Figure 4b presents the results of the elemental composition of the layer.

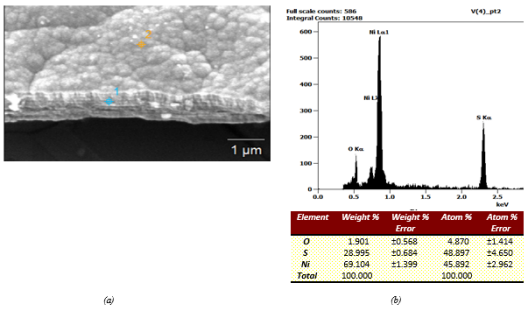

Element	Weight %	Weight % Error	Atom %	Atom % Error
O	1.901	±0.568	4.870	±1.414
S	28.995	±0.684	48.897	±4.650
Ni	69.104	±1.399	46.892	±2.962
Total	100.000		100.000	

(a) (b)

Fig. 4. *EDX microanalysis of Synthesis 1. (a). Points analyzed on the electrodeposited surface. (b). Composition of the layer. Source: own elaboration.*

The semiquantitative analysis showed a Ni/S atomic ratio close to 1:1, which suggests a composition compatible with a nickel sulfide of the NiS type$_x$. However, this assignment should be considered approximate, since EDX allows the local elemental proportion to be identified and estimated, but does not by itself confirm the crystalline phase of the material. Therefore, identifying specific nickel sulfide phases would require complementary structural characterization, such as X-ray diffraction, XRD[17],[20],[25],[30].

Figure 5 presents the morphological characterization of the coating obtained by synthesis 2. Figure 5a shows the nickel foam coated with NiS_x. This micrograph was acquired with an accelerating voltage of 20.00 kV at a magnification of 200x and a probe current of 1.6 *nA*.

Figure 5b shows the NiS_x coating deposited on the nickel foam. The micrograph was acquired with an accelerating voltage of 20.00 kV, a magnification of 1000x and a probe current of 1.6 nA. The image shows a relatively continuous layer on the substrate, with cracked areas that allowed the cross section of the coating to be observed and its thickness to be estimated.

Figure 5c presents the surface morphology of the coating, obtained with an accelerating voltage of 5.00 kV, a magnification of 20,000× and a probe current of 0.2 nA. The surface shows a heterogeneous morphology, associated with the growth of granular structures on the electrodeposited layer. Figure 5d presents a close-up of a fractured area of the NiS_x coating, acquired with an accelerating voltage of 5.00 kV, a magnification of 30,000x and a probe current of 25 pA. Synthesis 2 generated a cauliflower-like morphology, with an approximate average thickness of 880 nm and granular substructures close to 700 nm.

In addition, Figure 5c shows a close-up of the cauliflower-like structures formed during the electrodeposition. This micrograph was acquired with an accelerating voltage of 5.00 kV and a magnification of 25,000×. The cauliflower-like structures had an approximate average diameter of 3 µm.

Figure 6a, in turn, identifies the granular substructures that make up these morphologies, with average sizes close to 700 nm. This distinction allows the overall dimension of the cauliflower-like structure to be differentiated from the size of the granular units that compose it. Figure 6b shows the cross section of the coating obtained by synthesis 2. This micrograph shows that during the two electrodeposition steps, sublayers with differentiated morphologies formed on the nickel foam. The first step, corresponding to a current density of 10 mA cm^{-2}, produced a sublayer with predominantly columnar growth. The second step, corresponding to 100 mA cm^{-2}, formed a sublayer with coarser grains, associated with the cauliflower-like morphology

observed on the surface. The sublayer formed during the second step was thicker than the one obtained during the first step, despite having been deposited for a shorter time.

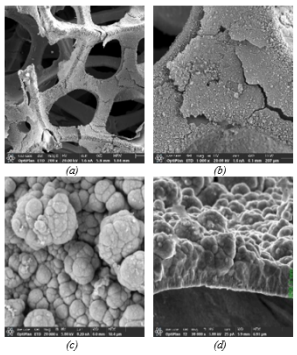

Fig. 5. *Synthesis 2. (a). Nickel foam coated with NiSx, (b). NiSx layer, (c). Surface morphology of NiSx. (d). Thickness of the NiSx layer. Source: own elaboration.*

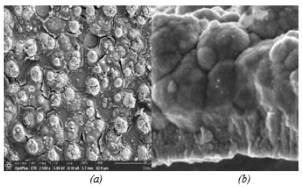

Fig. 6. *Cross-sectional view of the NiSx layer from synthesis 2. Source: own elaboration.*

Finally, microanalysis was performed by energy-dispersive X-ray spectroscopy, EDX, on the coating obtained by synthesis 2, as shown in Figure 7. The analysis was carried out in representative regions of the film, including an area located in the cross section of the sublayers formed during electrodeposition and another on the coating surface. Figure 7a shows the points selected for EDX analysis, while Figure 7b presents the elemental composition results obtained.

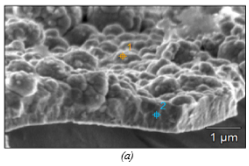

(a)

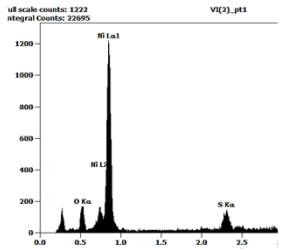

Element	Weight %	Weight % Error	Atom %	Atom % Error
O	3.789	±0.284	11.165	±2.511
S	17.338	±0.703	25.497	±3.102
Ni	78.873	±0.937	63.338	±2.257
Total	100.000		100.000	

(b)

Fig. 7. *EDX microanalysis of Synthesis 2. (a). Points analyzed on the electrodeposited surface. (b). Composition of the layer.*

The semiquantitative analysis revealed a Ni/S atomic ratio close to 2.5:1, indicating a coating enriched in nickel relative to synthesis 1. However, this ratio should be interpreted as a local compositional estimate, since the EDX technique alone cannot confirm the crystalline phase of the nickel sulfide formed. Such confirmation would require complementing the analysis with structural techniques, such as X-ray diffraction, XRD.

The comparison between both electrodeposition routes shows that the deposition conditions simultaneously modified the morphology, thickness and Ni/S ratio of the coating. Synthesis 1 produced a film with lamellar growth, an average thickness close to 720 nm and a Ni/S ratio close to 1:1. In contrast, synthesis 2 generated a cauliflower-like morphology, an average thickness close to 880 nm and an approximate Ni/S ratio of 2.5:1. These results indicate that the increase in current density

in the second route favored faster growth and a composition richer in nickel, which may be associated with differences in reduction kinetics, mass transport and local availability of sulfur species during electrodeposition.

The presence of oxygen detected by EDX should be interpreted as a surface signal associated with the chemical and environmental state of the coating, rather than as direct evidence of a specific crystalline phase. In synthesis 1 an oxygen content of 4.870 at.% was obtained, whereas in synthesis 2 this value increased to 11.165 at.%. This difference may be related to a greater surface exposure of the cauliflower-like morphology obtained in synthesis 2, which favors the adsorption of oxygenated species, moisture or surface residues after washing and drying. Additionally, the presence of oxygen may be associated with surface oxidation processes of nickel or nickel sulfides during drying and storage in air, as well as with the possible formation of hydroxide- or oxyhydroxide-type species on the surface.

It should also be considered that EDX analysis is semiquantitative and sensitive to the selected area, so these values should be interpreted as local compositional information. Consequently, the precise identification of oxides, hydroxides or oxyhydroxides would require complementary techniques, such as XRD, XPS or Raman spectroscopy.

CONCLUSIONS

Nickel sulfide coatings, NiS_x, were obtained on nickel foam by means of two electrodeposition routes. Synthesis 1, carried out by cyclic potentiodynamic electrodeposition, produced a film with a fine-grained surface morphology and rounded geometry. In the cross section, lamellar growth was observed, with sublayers associated with the applied electrodeposition cycles.

Synthesis 2, developed by means of two current density steps, generated a coating with a cauliflower-like morphology. Cross-sectional analysis revealed differences between the sublayers formed during each step: in the first step, corresponding to 10 mA cm^{-2}, predominantly columnar growth was observed, whereas in the second step, corresponding to 100 mA cm^{-2}, a coarser-grained sublayer associated with the cauliflower-like morphology was formed. These results indicate that the increase in current density favored significant changes in the surface morphology and coating thickness.

EDX microanalysis revealed the presence of nickel and sulfur in the coatings obtained by both synthesis routes. In synthesis 1, a Ni/S atomic ratio close to 1:1 was obtained, whereas in synthesis 2 this ratio was approximately 2.5:1, which indicates compositional differences associated with the electrodeposition conditions. However, because EDX provides semiquantitative elemental information, the identification of specific crystalline nickel sulfide phases requires complementary structural characterization, such as X-ray diffraction.

Overall, the results show that the electrodeposition conditions directly influence the surface morphology, cross-sectional growth, thickness and elemental Ni/S ratio of the NiS_x films deposited on nickel foam. This study provides experimental information useful for the design and optimization of nickel sulfide coatings on conductive porous substrates, as a preliminary step prior to future structural and electrochemical evaluations.

As a limitation of the study, it is noted that the characterization performed was restricted to morphological and compositional analysis by FESEM and EDX. Therefore, the specific crystalline phase of the coatings is not confirmed, nor is their electrochemical performance evaluated. In future work, it is recommended that these results be complemented with XRD, XPS or Raman, as well as with electrochemical techniques such as voltammetry, electrochemical impedance, polarization curves and stability tests.

REFERENCES

[1] J. Mohammed-Ibrahim and H. Moussab, “Recent advances on hydrogen production through seawater electrolysis,” *Mater. Sci. Energy Technol.*, vol. 3, pp. 780–807, Jan. 2020, doi: 10.1016/j.mset.2020.09.005.

[2] R. Li et al., “Electrodeposition: Synthesis of advanced transition metal-based catalyst for hydrogen production via electrolysis of water,” *Journal of Energy Chemistry*, vol. 57. Elsevier B.V., pp. 547–566, Jun. 01, 2021. doi: 10.1016/j.jechem.2020.08.040.

[3] Y. Yang et al., “The in-situ construction of NiFe sulfide with nanoarray structure on nickel foam as efficient bifunctional electrocatalysts for overall water splitting,” *J. Alloys Compd.*, vol. 874, Sep. 2021, doi: 10.1016/j.jallcom.2021.159874.

[4] H. Y. Wang et al., “Synergistically enhanced activity and stability of bifunctional nickel phosphide/sulfide heterointerface electrodes for direct alkaline seawater electrolysis,” *J. Energy Chem.*, vol. 75, pp. 66–73, Dec. 2022, doi: 10.1016/j.jechem.2022.08.019.

[5] A. Higareda, D. L. Hernández-Arellano, L. C. Ordoñez, R. Barbosa, and N. Alonso-Vante, “Advanced Electrocatalysts for the Oxygen Evolution Reaction: From Single- to Multielement Materials,” *Catalysts*, vol. 13, no. 10. Multidisciplinary Digital Publishing Institute (MDPI), Oct. 01, 2023. doi: 10.3390/catal13101346.

[6] T. Reier, H. N. Nong, D. Teschner, R. Schlögl, and P. Strasser, “Electrocatalytic Oxygen Evolution Reaction in Acidic Environments – Reaction Mechanisms and Catalysts,” *Advanced Energy Materials*, vol. 7, no. 1. Wiley-VCH Verlag, Jan. 11, 2017. doi: 10.1002/aenm.201601275.

[7] Z. Yan, H. Liu, Z. Hao, M. Yu, X. Chen, and J. Chen, “Electrodeposition of (hydro)oxides for an oxygen evolution electrode,” *Chemical*

Science, vol. 11, no. 39. Royal Society of Chemistry, pp. 10614–10625, Oct. 21, 2020. doi: 10.1039/d0sc01532f.

[8] J. Rossmeisl, A. Logadottir, and J. K. Nørskov, "Electrolysis of water on (oxidized) metal surfaces," *Chem. Phys.*, vol. 319, no. 1–3, pp. 178–184, Dec. 2005, doi: 10.1016/j.chemphys.2005.05.038.

[9] F. Song et al., "Transition Metal Oxides as Electrocatalysts for the Oxygen Evolution Reaction in Alkaline Solutions: An Application-Inspired Renaissance," *J. Am. Chem. Soc.*, vol. 140, no. 25, pp. 7748–7759, Jun. 2018, doi: 10.1021/jacs.8b04546.

[10] J. W. D. Ng et al., "Gold-supported cerium-doped NiOx catalysts for water oxidation," *Nat. Energy*, vol. 1, no. 5, p. 16053, Apr. 2016, doi: 10.1038/nenergy.2016.53.

[11] S. Jiang et al., "Recent Advances in Seawater Electrolysis," *Catalysts*, vol. 12, no. 2. MDPI, Feb. 01, 2022. doi: 10.3390/catal12020123.

[12] L. An et al., "Recent Development of Oxygen Evolution Electrocatalysts in Acidic Environment," *Adv. Mater.*, vol. 33, no. 20, May 2021, doi: 10.1002/adma.202006328.

[13] B. Zhang et al., "Homogeneously dispersed multimetal oxygen-evolving catalysts." [Online]. Available: https://www.science.org

[14] M. S. Burke, M. G. Kast, L. Trotochaud, A. M. Smith, and S. W. Boettcher, "Cobalt-Iron (Oxy)hydroxide Oxygen Evolution Electrocatalysts: The Role of Structure and Composition on Activity, Stability, and Mechanism," *J. Am. Chem. Soc.*, vol. 137, no. 10, pp. 3638–3648, Mar. 2015, doi: 10.1021/jacs.5b00281.

[15] X. Lu and C. Zhao, "Electrodeposition of hierarchically structured three-dimensional nickel-iron electrodes for efficient oxygen evolution at high current densities," *Nat. Commun.*, vol. 6, Mar. 2015, doi: 10.1038/ncomms7616.

[16] B. Zhang et al., "High Corrosion Resistance of NiFe-Layered Double Hydroxide Catalyst for Stable Seawater Electrolysis Promoted by Phosphate Intercalation," *Small*, vol. 18, no. 45, Nov. 2022, doi: 10.1002/smll.202203852.

[17] Y. Li, T. Dai, Q. Wu, X. Lang, L. Zhao, and Q. Jiang, "Design heterostructure of NiS–NiS2 on NiFe layered double hydroxide with Mo doping for efficient overall water splitting," *Mater. Today Energy*, vol. 23, Jan. 2022, doi: 10.1016/j.mtener.2021.100906.

[18] C. G. Morales-Guio, L. Liardet, and X. Hu, "Oxidatively Electrodeposited Thin-Film Transition Metal (Oxy)hydroxides as Oxygen Evolution Catalysts," *J. Am. Chem. Soc.*, vol. 138, no. 28, pp. 8946–8957, Jul. 2016, doi: 10.1021/jacs.6b05196.

[19] F. Calle-Vallejo, O. A. Díaz-Morales, M. J. Kolb, and M. T. M. Koper, "Why is bulk thermochemistry a good descriptor for the electrocatalytic activity of transition metal oxides?," *ACS Catal.*, vol. 5, no. 2, pp. 869–873, Feb. 2015, doi: 10.1021/cs5016657.

[20] B. Cui et al., "Heterogeneous lamellar-edged Fe-Ni(OH)2/Ni3S2 nanoarray for efficient and stable seawater oxidation," *Nano Res.*, vol. 14, no. 4, pp. 1149–1155, Apr. 2021, doi: 10.1007/s12274-020-3164-3.

[21] A. R. Jadhav et al., "Stable complete seawater electrolysis by using interfacial chloride ion blocking layer on catalyst surface," *J. Mater. Chem. A*, vol. 8, no. 46, pp. 24501–24514, Dec. 2020, doi: 10.1039/d0ta08543j.

[22] F. Dionigi, T. Reier, Z. Pawolek, M. Gliech, and P. Strasser, "Design Criteria, Operating Conditions, and Nickel-Iron Hydroxide Catalyst Materials for Selective Seawater Electrolysis," *ChemSusChem*, vol. 9, no. 9, pp. 962–972, May 2016, doi: 10.1002/cssc.201501581.

[23] S. H. Hsu et al., "An Earth-Abundant Catalyst-Based Seawater Photoelectrolysis System with 17.9% Solar-to-Hydrogen Efficiency," *Adv. Mater.*, vol. 30, no. 18, May 2018, doi: 10.1002/adma.201707261.

[24] Y. Kuang et al., "Solar-driven, highly sustained splitting of seawater into hydrogen and oxygen fuels," *Proc. Natl. Acad. Sci. U. S. A.*, vol. 116, no. 14, pp. 6624–6629, Apr. 2019, doi: 10.1073/pnas.1900556116.

[25] J. Lin et al., "Defect-Rich Heterogeneous MoS2/NiS2 Nanosheets Electrocatalysts for Efficient Overall Water Splitting," *Adv. Sci.*, vol. 6, no. 14, Jul. 2019, doi: 10.1002/advs.201900246.

[26] Y. Fang et al., "Experiments combined with theoretical research on the effect of hydrogen evolution by the nanosheet of NiS–CdS–CN catalyst," *Int. J. Hydrogen Energy*, vol. 47, no. 12, pp. 7724–7737, Feb. 2022, doi: 10.1016/j.ijhydene.2021.12.098.

[27] K. Share, J. Lewis, L. Oakes, R. E. Carter, A. P. Cohn, and C. L. Pint, "Tungsten diselenide (WSe2) as a high capacity, low overpotential conversion electrode for sodium ion batteries," *RSC Adv.*, vol. 5, no. 123, pp. 101262–101267, 2015, doi: 10.1039/c5ra19717a.

[28] Z. Kato, N. Kumagai, K. Asami, and K. Hashimoto, "The Effect of Tungsten Addition to the Intermediate IrO2 Layer of Mn-Mo-O/IrO2/Ti Electrodes on the Performance for Oxygen Evolution in Seawater Electrolysis," *ECS Meet. Abstr.*, vol. MA2005-02, no. 8, pp. 377–377, 2006, doi: 10.1149/ma2005-02/8/377.

[29] D. Zhou et al., "Layered double hydroxide-based electrocatalysts for the oxygen evolution reaction: Identification and tailoring of active sites, and superaerophobic nanoarray electrode assembly," *Chemical Society Reviews*, vol. 50, no. 15. Royal Society of Chemistry, pp. 8790–8817, Aug. 07, 2021. doi: 10.1039/d1cs00186h.

[30] G. Zhang et al., "Design and construction of hierarchical Ni3S2 @V-doped NiMn-LDH heterostructure on rGO/Ni foam as an advanced electrode for battery-supercapacitor hybrid devices," *J. Alloys Compd.*, vol. 896, Mar. 2022, doi: 10.1016/j.jallcom.2021.163125.

[31] W. D. Chemelewski, H. C. Lee, J. F. Lin, A. J. Bard, and C. B. Mullins, "Amorphous FeOOH oxygen evolution reaction catalyst for photoelectrochemical water splitting," *J. Am. Chem. Soc.*, vol. 136, no. 7, pp. 2843–2850, Feb. 2014, doi: 10.1021/ja411835a.

[32] Marisol Soledad Maril Millán, "Desarrollo de un ánodo electrocatalítico para electrólisis de agua de mar," 2022.

[33] Rodríguez Rodríguez Jordi, "Síntesis y Caracterización de Óxido de Grafeno Reducido Funcionalizado con Nanopartículas Metálicas. Aplicación en el Desarrollo de Sensores Amperométricos Basados en Materiales Nanoestructurados," 2020.

[34] C. Wang, Y. Wu, Z. Zhou, J. Wang, S. Pei, and S. Liu, "Electrodeposited amorphous nickel–iron phosphide and sulfide derived films for electrocatalytic oxygen evolution," *Int. J. Hydrogen Energy*, vol. 47, no. 97, pp. 40849–40859, 2022, doi: 10.1016/j.ijhydene.2022.09.200.

[35] M. J. Kenney et al., "An electrodeposition approach to metal/metal oxide heterostructures for active hydrogen evolution catalysts in

near-neutral electrolytes," Nano Res., 2019, doi: 10.1007/s12274-019-2379-7.

ACKNOWLEDGMENTS

The authors thank Universidad de Antioquia for the support provided during their doctoral training, within the framework of which this research was developed. They also thank Universidad Militar Nueva Granada (UMNG) for the academic conditions that facilitated the partial preparation of this manuscript during their affiliation with the institution.

FUNDING

Universidad de Antioquia funded the doctoral studies of Claudia Patricia Parra Medina, from which this work is derived, through the Beca Fondo Doctoral UdeA awarded in 2022.

CONFLICT OF INTEREST

None

AUTHORSHIP CONTRIBUTIONS

Drafting – original draft: Claudia Patricia Parra Medina, Edwin García Quintero, Héctor Darío Sánchez Londoño.

Writing–review and editing: Claudia Patricia Parra Medina, Edwin García Quintero, Héctor Darío Sánchez Londoño.